Fibers and Polymers 2005, Vol.6, No.3, 186-199

An in Depth Study of Crystallinity, Crystallite Size and Orientation Measurements of a Selection of Poly(Ethylene Terephthalate) Fibers

Ismail Karacan*

Department of Textile Engineering, Faculty of Engineering, Erciyes University, TR-38039 Kayseri-Turkey
(Received January 25, 2005; Revised April 11, 2005; Accepted July 22, 2005)

Abstract: A selection of commercially available poly(ethylene terephthalate) fibers with different degrees of molecular alignment and crystallinity have been investigated utilizing a wide range of techniques including optical microscopy, infrared spectroscopy together with thermal and wide-angle X-ray diffraction techniques. Annealing experiments showed increased molecular alignment and crystallinity as shown by the increased values of birefringence and melting enthalpies. Crystallinity values determined from thermal analysis, density, unpolarized infrared spectroscopy and X-ray diffraction are compared and discussed in terms of the inherent capabilities and limitations of each measurement technique. The birefringence and refractive index values obtained from optical microscopy are found to decrease with increasing wavelength of light used in the experiments. The wide-angle X-ray diffraction analysis shows that the samples with relatively low orientation possess oriented non-crystalline array of chains whereas those with high molecular orientation possess well defined and oriented crystalline array of chains along the fiber axis direction. X-ray analysis showed increasing crystallite size trend with increasing molecular orientation. SEM images showed micro-cracks on low oriented fiber surfaces becoming smooth on highly oriented fiber surfaces. Excellent bending characteristics were observed with knotted fibers implying relatively easy fabric formation.

Keywords: Poly(ethylene terephthalate), Density, Crystallinity, Infrared spectroscopy, Thermal analysis, Birefringence, X-ray diffraction

Introduction

Commercially available polyester fibers are receiving increasing interest from academia and industry due to their desirable properties including ease of processibility, low cost, and good thermal behaviour. It is well established that operating speeds play an important role in the enhancement of mechanical properties through increased degree of order and alignment of polymer chains along the fiber axis direction. As a result, a full understanding of molecular structure of industrially important poly(ethylene terephthalate) fibers is of paramount importance for our improved understanding of processing-structure-property relationships.

Due to its commercial importance, molecular structure of polyester has been the subject of many interesting and useful investigations mainly using a wide range of techniques including infrared [1-8] and Raman[9-11] spectroscopy, X-ray diffraction [12-14], NMR [15], and Transmission Electron Microscopy [16]. Ward and co-workers working on fibers and uniaxially and biaxially oriented polyester films developed the theoretical considerations and their applications behind the use of polarized infrared [1-3] and Raman spectroscopy [13, 14,16,19] techniques in the quantitative characterization of orientation parameters. Zhang *et al.* working on the ultra-thin PET films showed the variation of crystallinity values with variations in film thickness values during isother crystallization [7,8]. They attributed the reduction in crystallinity with decreasing film thickness to slower crystallization taking place during crystallization stages. Orientation measurements also showed significant thickness dependence [8]. Bower and Ward showed the presence of polarization scrambling during the fiber orientation measurements using Raman spectroscopy [11]. They obtained good results by immersing the fibers in liquid of refractive index equal to the mean fiber refractive index.

Although the early measurements of crystallinity [12] were based on arbitrary separation of crystalline and non-crystalline components, nowadays computational procedures are successfully used to resolve the overlapping X-ray diffraction profiles to evaluate quantitative structural parameters [13]. More recently, Yoshioka *et al.* produced uniaxially oriented films of poly (ethyelene terephthalate) and poly(ethylene 2,6-naphthalene dicarboxylate) and their blends [16]. They studied the resulting morphologies with transmission electron microscopy. Using selected area electron diffraction, it was shown that the polymer chains form uniaxial orientation.

In the present investigation, commercially available poly (ethyelene terephthalate) fibers have been studied in terms of the degree of crystallinity, crystallite size, and orientation measurements using a wide range of techniques with the ultimate aim of gaining an enhanced understanding of the processing-structure-property relationships.

Experimental

Materials

Totally six original and five annealed samples of PET fibers commercially produced by Polyteks A.S. of Turkey were investigated. Details of the samples showing the linear density, number of filaments, decitex per filament, and density

*Corresponding author: ismailkaracan@erciyes.edu.tr

Table 1. Sample details

Sample	Comments	Linear density (dtex)	No. of filaments	dtex/filament	Density from isotropic refractive indices, ρ (g/cm^3)
S1	Medium oriented yarn	78	128	0.609	1.3727
S2	Partially oriented yarn	78	128	0.609	1.3751
S3	Fully oriented yarn	78	24	3.350	1.3863
S4	Fully drawn yarn	78	128	0.609	1.3930
S5	Intermingled yarn	78	128	0.609	1.3973
S6	Air-textured yarn	167	256	0.652	1.3845

are listed in Table 1. Due to the commercial reasons, the processing conditions are not released, therefore, the samples are referred to by their commercial names. A stainless steel frame with dimensions of 300 mm × 300 mm was constructed to carry out the annealing experiments. The samples were kept under optimum tension during the experiments with the aim of preventing the possible shrinkage. Each sample was annealed in a pre-heated oven, in air, at 160 °C for the annealing times between 1 and 120 hrs, respectively.

Refractive Index Measurements

The refractive indices of the fiber samples with the aim of determining birefringence values were measured using an image splitting Carl Zeiss Jena interphako interference microscope. The measurements of refractive indices were carried out for wavelengths of 486.1, 546.1, 551, 589.3, and 656.3 nm, respectively. The refractive indices in the fiber axis direction ($n_{//}$) and transverse direction ($n_{\perp}$) were measured by matching the refractive index of Cargille immersion liquids. The measured values of the refractive indices and the birefringences are shown in Tables 2 and 3.

Infrared Measurements

An IR-Plan® microscope installed on a Nicolet Magna IR 750 Fourier Transform spectrophotometer was employed for infrared measurements. The IR-plan® microscope allows the single fibers to be examined. On an average 10 single filaments were studied to maintain the reproducibility of the results. In all cases, 200 interferograms of a sample were averaged and transformed with Happ-Genzel apodization function. All the spectra were collected at a resolution of 2 cm^{-1}. Finally, all the spectra were analyzed by curve fitting procedures [19] to obtain accurate peak parameters.

DSC Measurements

The differential scanning calorimetry (DSC) experiments were carried out using a DuPont Differential Scanning Calorimeter controlled by a Thermal Analyst 2000 system. Typical sample weights used were approximately 5 mg. The heating rate of 10 °C/min and an upper temperature range of 300 °C were selected. Indium (m.p. 156.5 °C) was used as calibration standard. The specimens were always tested in a nitrogen environment. The fiber samples were cut in very

Table 2. Birefringence and optical orientation parameters of PET fiber samples

Sample	$n_{\parallel}$ at 551 nm	$n_{\perp}$ at 551 nm	n_{iso} at 551 nm	Δn at 551 nm	$\langle P_{200}\rangle_{opt}$	$\langle\cos^2\theta_{c,f}\rangle_{opt}$	Orientation angle (°) $\langle\theta_{c,f}\rangle_{opt}$
S1	1.663	1.560	1.594	0.103	0.430	0.620	38.06
S2	1.667	1.559	1.595	0.108	0.452	0.635	37.17
S3	1.683	1.560	1.601	0.123	0.508	0.672	34.94
S4	1.698	1.558	1.6046	0.140	0.574	0.716	32.20
S5	1.702	1.560	1.607	0.142	0.579	0.719	32.01
S6	1.698	1.552	1.600	0.146	0.604	0.736	30.92

Table 3. Birefringence, density and optical orientation parameters of annealed fiber samples

Annealing time	$n_{\parallel}$ at 551 nm	$n_{\perp}$ at 551 nm	Δn at 551 nm	Density ρ (g/cm^3)	$\langle P_{200}\rangle_{opt}$	$\langle\cos^2\theta_{c,f}\rangle_{opt}$	Orientation angle (°) $\langle\theta_{c,f}\rangle_{opt}$
unannealed	1.667	1.559	0.108	1.3751	0.452	0.635	37.17
1 hour	1.698	1.552	0.146	1.3845	0.611	0.741	30.62
2 hours	1.698	1.553	0.145	1.3863	0.605	0.737	30.86
5 hours	1.707	1.552	0.155	1.3921	0.643	0.762	29.20
7.5 hours	1.703	1.560	0.143	1.3973	0.590	0.726	31.54
120 hours	1.699	1.560	0.139	1.3963	0.574	0.716	32.20

short lengths, placed into an aluminium pan and sealed with a lid. An empty pan sealed with a lid was used as a reference.

X-ray Diffraction

Wide-angle X-ray diffraction patters were recorded on a flat plate at a sample to camera distance of 5 cm. The wide-angle X-ray traces were obtained using Phillips X-ray diffractometer system utilizing nickel filtered CuK_α radiation (wavelength of 0.1542 nm) and voltage and current settings of 10 kV and 30 mA, respectively. Counting was carried out at 20 steps per degree. The observed equatorial X-ray scattering data in the 2θ= 10-35 ° range was corrected and resolved using a well established curve fitting procedure [19]. The peak widths at half-height have been corrected using the Stoke's deconvolution procedure [20]. Finally, the apparent crystallite size of a given reflection was evaluated using the Scherrer equation:

$$L_{(hkl)} = \frac{K \cdot \lambda}{\beta \cdot \cos(\theta)} \quad (1)$$

where θ is the Bragg angle for the reflection concerned, λ is the wavelength of radiation (0.1542 nm), $L_{(hkl)}$ is the mean length of the crystallite perpendicular to the planes (*hkl*), β is either the integral breadth or the breadth at half maximum intensity in radians and K is a Scherrer parameter.

Analysis of Experimental Data

Infrared Data-Curve Fitting

The unpolarized infrared spectra of poly(ethylene terephthalate) fiber samples in the 1190-930 cm^{-1} region were curve-fitted according to an established procedure described previously [19]. During the curve-fitting procedures, it was found necessary to include the peaks at 1030 and 1102 cm^{-1} to improve the fits in the tails of the major peaks, but they are not considered any further. During the IR data collection, an average of 10 single filaments were tested to maintain the reproducibility of the results.

Evaluation of Orientation Averages from Refractive Indices

For a transversely isotropic sample, such as uniaxially oriented fiber, the measured refractive indices can be used to calculate optical orientation averages by using the following general equations [1,2,17,18].

$$\frac{\phi_{||} - \phi_\perp}{\phi_{||} + 2\phi_\perp} = \frac{2\Delta\alpha}{3\alpha_0} P_{200} \quad (2)$$

$$\text{where } \phi_i = \frac{n_i^2 - 1}{n_i^2 + 2} \quad (3)$$

Substituting the expressions for ϕ_i (where i is || or ⊥) from equation (3) into equation (2) and writing $\Delta n = n_{||} - n_\perp$ and $n_{iso} = 1/3(n_{||} + 2n_\perp)$ then leads, to a good approximation, to

$$P_{200} = \left(\frac{3\alpha_0}{\Delta\alpha}\right) \frac{2n_{iso}\Delta n}{(n_{iso}^4 + n_{iso}^2 - 2)} \quad (4)$$

where Δn is the birefringence, $n_{||}$ is the refractive index parallel to the fiber axis direction, $n_\perp$ is the refractive index perpendicular to the fiber axis direction and n_{iso} the isotropic refractive index. In the present study, a value of 0.24 has been used as the maximum birefringence value for the fully oriented sample of poly(ethylene terephthalate) [21]. Substituting $P_{200} = 1$ in equation (4), together with the experimental value of n_{iso}, leads to $3\alpha_0/\Delta\alpha = 9.2 \pm 0.2$. For the annealed samples, the value of $3\alpha_0/\Delta\alpha$ is found to be 9.3 ± 0.2. Using these values and equation (4), the values of P_{200} can be determined from the refractive index data shown in Tables 2 and 3. The P_{200} is known as the Herman's orientation factor in the polymer and fiber science. From P_{200}, the values of $<\cos^2\theta_{c,f}>_{opt}$ can be determined using equation (5), and the results for the samples are shown in Tables 2 and 3.

$$<\cos^2\theta_{c,f}>_{opt} = \frac{1}{3}(1 + 2<P_{200}>) \quad (5)$$

From $<\cos^2\theta_{c,f}>_{opt}$, the values of orientation angle, $<\theta_{c,f}>_{opt}$, where $<\theta_{c,f}>_{opt}$ is the orientation angle between the chains and the fiber axis direction, can be calculated and the results are listed in Tables 2 and 3.

Evaluation of Density from Refractive Index Values

According to Vries [21], density (ρ) can be calculated using the relation in equation (6)

$$\rho = K\left[\frac{n_{iso}^2 - 1}{n_{iso}^2 + 2}\right] \quad (6)$$

where n_{iso} is defined as the isotropic refractive index determined from equation (7).

$$n_{iso} = \frac{1}{3}(n_{||} + 2n_\perp) \quad (7)$$

Using equations (6) and (7), the density of the PET fiber samples can be estimated. The constant K is given by Vries as 4.047 for PET samples [21]. The estimated density (ρ) values are listed in Tables 1 and 3.

Evaluation of Crystallinity from Density Values

Fractional crystallinity, using the density values evaluated from equation (6), can be determined using equation (8).

$$\chi_c = \frac{\rho - \rho_a}{\rho_c - \rho_a} \times 100(\%) \quad (8)$$

where ρ is the density of the sample evaluated using isotropic refractive index value for each sample and ρ_a is the density of the amorphous phase given as 1.335 g/cm^3 whereas ρ_c is the density of the fully crystalline material given as 1.455 g/

cm^3 by Daubeny *et al.* [22].

Evaluation of Crystallinity from Melting Enthalpy Values

Assuming a two-phase model consisting of crystalline and non-crystalline (i.e., amorphous) phase, the degree of crystallinity can be evaluated from the melting enthalpies using equation (9)

$$\chi_c = \frac{\Delta H_m}{\Delta H_m^0} \times 100(\%) \quad (9)$$

where χ_c is the degree of crystallinity evaluated by DSC method, ΔH_m is the melting enthalpy of the sample and ΔH_m^0 is the melting enthalpy of 100 % crystalline sample and is taken as 140 ± 20 J/g as published in the literature [23].

Sometimes, as-spun fibers, exhibit a small exothermic peak associated with crystallization. This implies incomplete crystallization during the as-spun fiber formation. As a result, the area of crystallization exotherm must be deducted from the area of melting endotherm to obtain the original corrected melting enthalphy. The melting enthalpy, should, therefore be re-evaluated as follows in equation (10)

$$\Delta H_m = \Delta H_2 - \Delta H_1 \quad (10)$$

where ΔH_2 is melting enthalpy and ΔH_1 is crystallization enthalpy.

Evaluation of Crystallinity from X-ray Diffraction Data

X-ray crystallinity [13] is based on the ratio of the integrated intensity under the resolved peaks (above the fitted baseline) to the integrated intensity of the total scatter under the experimental trace. This definition can be expressed as in equation (11).

$$\chi_c = \frac{\int_0^{2\pi} I_{cr}(2\theta)d(2\theta)}{\int_0^{2\pi} I_{tot}(2\theta)d(2\theta)} \quad (11)$$

The area under the background is considered to correspond to the non-crystalline scatter. It should be emphasized that X-ray crystallinity is defined between two arbitrarily chosen angles and should be considered as an optimum mathematical solution. In this work, the peak area crystallinity was estimated in the 2θ range between 10 and 35 °.

Evaluation of Crystallinity from Infrared Spectroscopy

The infrared crystallinity value of the samples is determined using the 973 and 1018 cm^{-1} IR bands using the equation (12)

$$\chi_{c(\text{i.r.})} = \frac{A_{973}}{A_{1018}} \times 100(\%) \quad (12)$$

where A_{973} and A_{1018} are the absorbance values of the infrared bands located at 973 and 1018 cm^{-1}, respectively. Unpolarized spectrum was used for the infrared crystallinity calculations due to the orientation independent data requirement.

Results and Discussion

In the textile industry, the melt-spun polyester yarns are classified according to the degree of orientation incorporated through different operating speeds introduced during the fiber formation stages. Normally operating speeds of 500 to 1500 m/min give *low oriented yarn*, whereas the processing speeds of 1500 to 2500 m/min give *medium oriented yarn*. Yarns referred to as *partially oriented yarn* are produced with operating speeds between 2500 and 4000 m/min. Between 4000 and 6000 m/min, *highly oriented yarn* can be obtained. Finally, *fully oriented yarn* is produced with processing speeds above 6000 m/min. The intention behind the use of increasing operating speeds is to produce fibers with enhanced tensile properties via increased degree of alignment of chains along the fiber axis direction. The melt-spun poly(ethylene terephthalate) yarns produced with different degrees of alignment through different operating speeds are listed in Table 1 with their commercial identification names.

The melt-spun polyester yarns are textured to give the characteristics of natural staple fibers via the introduction of increased bulk or mass incorporating crimps, coils or loops along the length of the filaments. In principle, air-texturing uses a cold air stream to produce entangled bulky yarns involving the overfeeding a yarn into a turbulent air-jet to form excess length into loops [24] as shown in Figure 1, whereas the intermingling process involves the introduction of mingling process using cold air-jets to create turbulence to entangle the continuous filament yarns during, for example in high speed spin-drawing, high-speed take-up or the false-twisting stage to impart cohesion to the yarn without forming loops as shown in Figure 2.

Annealing is usually carried out to release internal stresses and strains taking place during the fiber formation while causing greater dimensional stability, reduction or elimination

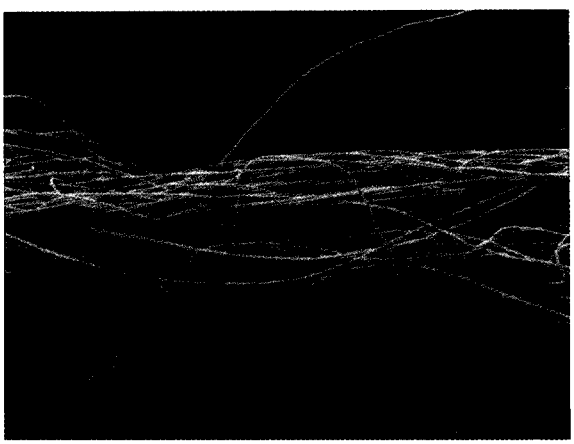

Figure 1. Longitudinal SEM image of air-textured poly(ethylene terephthalate) yarn (×72).

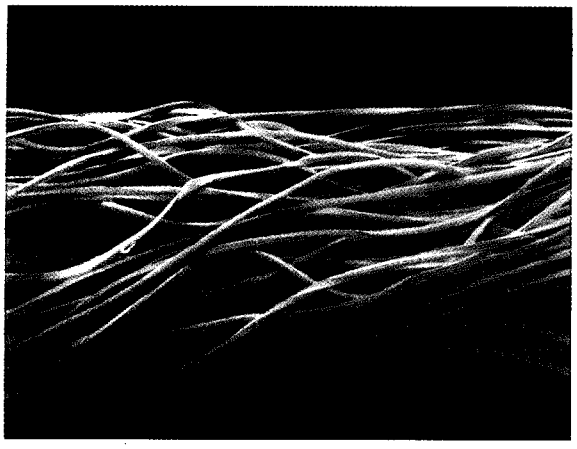

Figure 2. Longitudinal SEM image of intermingled poly(ethylene terephthalate) yarn (×200).

of defects and improvement in mechanical properties [25].

Optical Microscopy Data

The refractive index values measured at 551 nm are listed in Tables 2 and 3. As shown in Figure 3, the refractive index values are found to decrease with increasing wavelength. The effects of annealing on birefringence are summarized in Table 3. It is clear that the birefringence, defined as a measure of overall orientation, shows a tendency to increase with increasing annealing time of up to 5 hours, when the *partially oriented yarn* samples are treated in constrained condition and then exhibits slight decrease after annealing times of 7.5 and 120 hours, possibly due to some molecular relaxation processes taking place with prolonged annealing times.

Evaluated optical orientation parameters in terms of Herman's orientation factor ($<P_{200}>_{opt}$), $<\cos^2\theta_{c,f}>_{opt}$ and orientation angle, $<\theta_{c,f}>_{opt}$, are summarized in Tables 2 and 3 for yarns produced with different processing speeds and for annealed samples. The results suggest that following the increasing processing speeds, the fibers are introduced with higher molecular orientation and a high degree of crystallinity. It shows that the average angle, $<\theta_{c,f}>_{opt}$, between the poly (ethylene terephthalate) chains and the fiber axis varies between 32.2° and 38.06° for the untextured samples. The orientation angles for the intermingled and air-textured samples are found to be 32.01° and 30.92°, respectively. In the case of the annealed samples, the orientation angle varies between 29.2° and 32.2°.

Thermal Analysis Data

The DSC traces of *medium oriented* (sample S1) and *partially oriented* (sample S2) melt-spun fibers shown in Figure 4 exhibit crystallization exotherms with peak temperatures of 118.3 °C and 109 °C, respectively, due to the effects of incomplete crystallization taking place during the fiber formation stages. The crystallization enthalpies for these samples have been subtracted from the melting enthalpies to obtain correct crystalllinity values listed in Tables 4 and 5. As shown in Figures 4 and 5, the melting temperatures of original melt-spun fibers produced with different processing speeds and hence with different molecular orientation values are found to vary between 253.5 and 261 °C, respectively. It

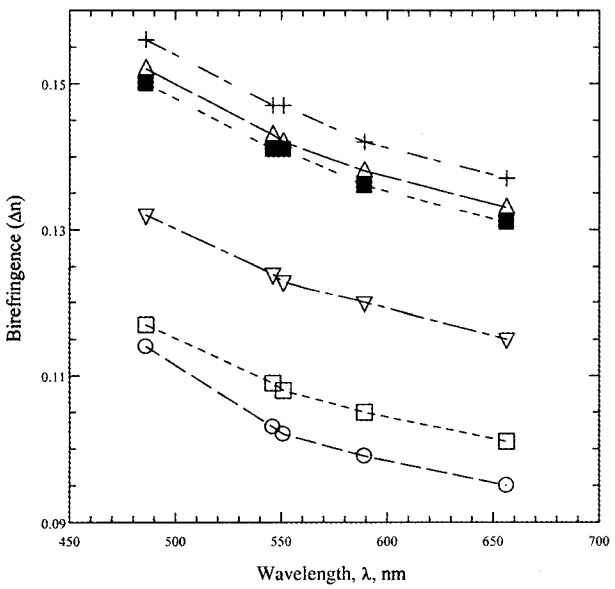

Figure 3. Variation of birefringence (Δn) with wavelength of light used in the experiments. (○) sample S1, (□) sample S2, (▽) sample S3, (■) sample S4, (△) sample S5, (+) sample S6. See Table 1 for sample definition.

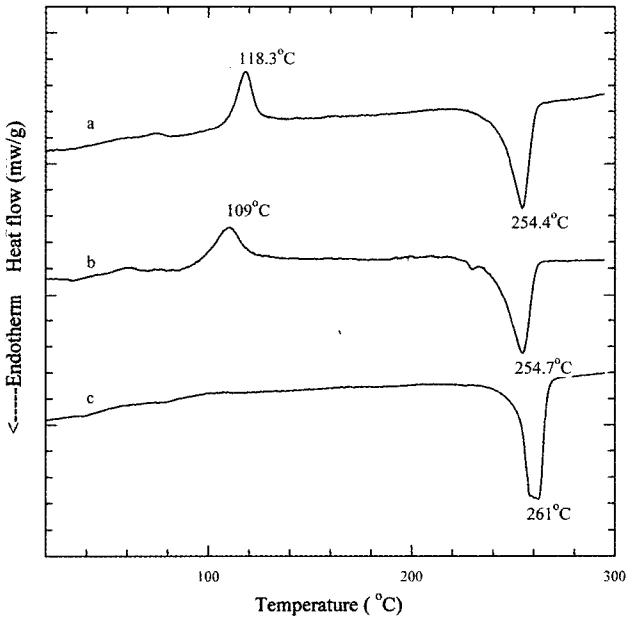

Figure 4. DSC thermograms of (a) sample S1, (b) sample S2 and (c) sample S3. Crystallization and melting temperatures are shown on the figures. See Table 1 for sample definition.

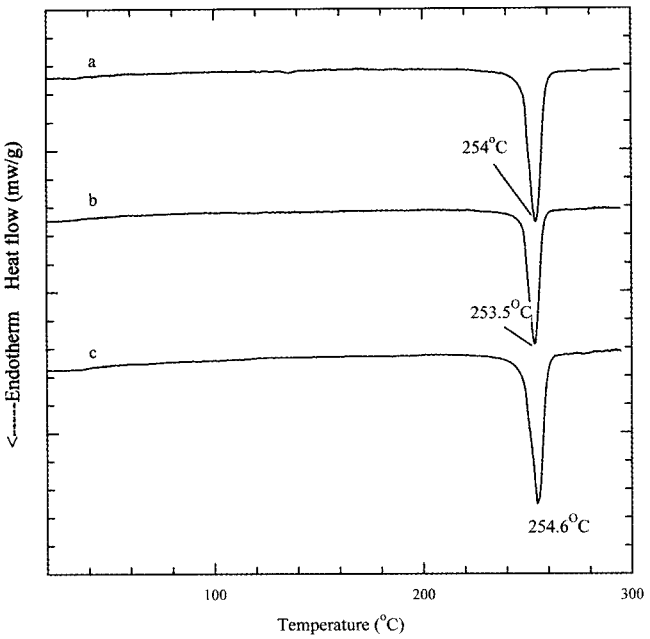

Figure 5. DSC thermograms of (a) sample S4, (b) sample S5 and (c) sample S6. Melting temperatures are shown on the figures. See Table 1 for sample definition.

Table 4. Thermal analysis results of original PET fiber samples

Sample	ΔH_1 (J/g) due to crystallization	ΔH_2 (J/g) due to melting	ΔH (J/g) corrected	DSC crystallinity χ_c(%)
S1	19.39	41.28	21.89	15.63
S2	16.68	40.99	24.31	17.36
S3	-	49.12	49.12	35.09
S4	-	57.20	57.20	40.86
S5	-	60.35	60.35	43.10
S6	-	56.42	56.42	40.30

Table 5. Thermal analysis results of annealed PET samples

Annealing time	ΔH_1 (J/g) due to crystallization	ΔH_2 (J/g) due to melting	ΔH (J/g) corrected	DSC crystallinity χ_c(%)
Unannealed	16.680	40.99	24.310	17.36
1 hour	3.034	53.91	50.876	36.34
2 hours	3.942	55.17	51.228	36.59
5 hours	5.243	55.19	49.947	35.68
7.5 hours	6.553	63.36	56.807	40.58
120 hours	4.565	61.24	56.675	40.48

is clear that increasing orientation has a distinct role with increasing melting temperatures and the disappearance of crystallization exothermic peaks due to the improved lateral

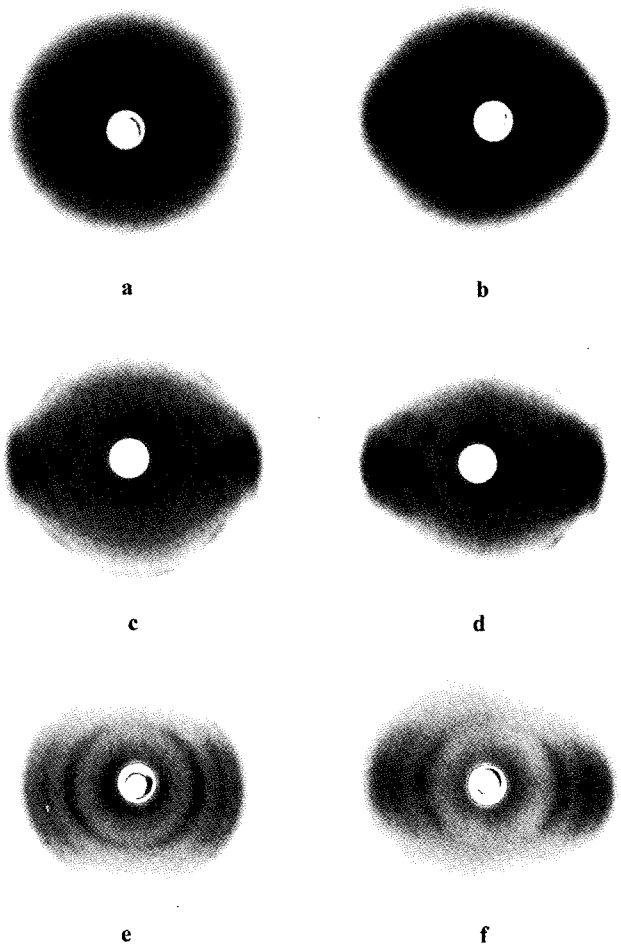

Figure 6. Wide-angle X-ray diffraction patterns of (a) sample S1, (b) sample S2, (c) sample S3, (d) sample S4, (e) sample S5, and (f) sample S6. Fiber axis is vertical. See Table 1 for sample definition.

perfection taking place along the fiber axis direction.

The results suggest a variation of DSC crystallinity 15.6 and 43.1 % as the alignment of polymer chains progresses with increasing processing speeds. As shown in Table 5, annealing causes increased amount of crystallinity of the parent sample from an initial DSC crystallinity of 17.4 % to 40.6 % for an annealing time of 7.5 hours.

Analysis of Wide-Angle X-Ray Diffraction Data

Structure of Untextured Melt-Spun Yarns with Low Orientation and Crystallinity

Qualitative inspection of WAXS pattern of *medium oriented* (sample S1) shown in Figure 6(a) shows a broad halo centred around $2\theta = 22°$ with considerable azimuthal spread to the meridional region. Equatorial trace shown in Figure 7(a) is found to be asymmetrical and can be resolved into at least three broad peaks labelled as PA1, PA2 and PA3, respectively.

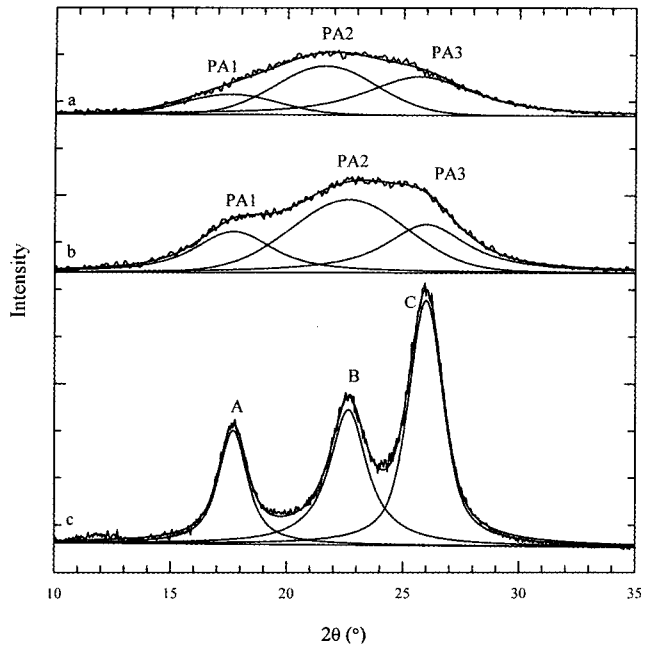

Figure 7. Resolved equatorial X-ray diffraction traces of (a) sample S1, (b) sample S2 and (c) sample S3. A: 010, B: $1\bar{1}0$, C: 100 peaks. See Table 1 for sample definition.

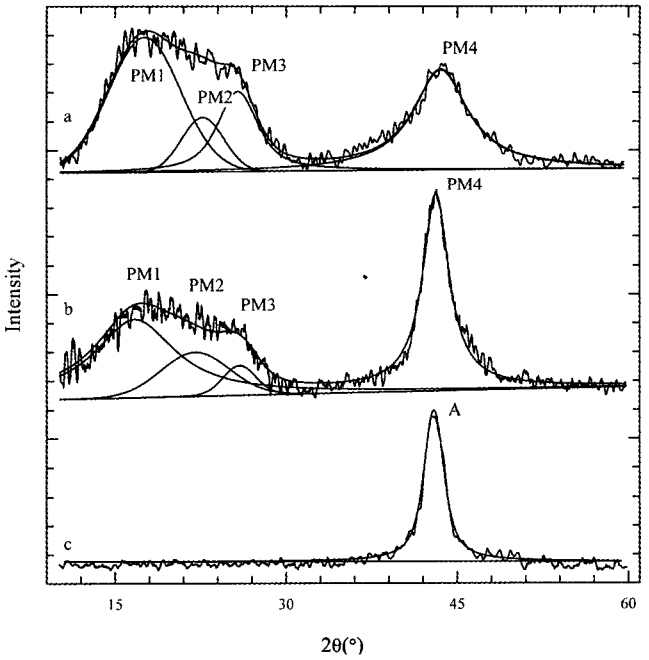

Figure 8. Resolved meridional X-ray diffraction traces of (a) sample S1, (b) sample S2 and (c) sample S3. A, extension of $\bar{1}05$ peak into the meridional region. See Table 1 for sample definition.

The corresponding *d*-spacings and half-height widths before and after instrumental broadening correction are summarized in Table 6. The results suggest a slightly oriented non-crystalline structure containing so called micro-crystallites consisting of

Table 6. Apparent crystallite sizes obtained from resolved equatorial X-ray diffraction traces

Sample	*hkl* indexing	Observed *d*-spacing (nm)	Experimental half-height width (2θ, deg)	Corrected half-height width (2θ, deg)	$L_{(hkl)}$ apparent crystallite size (nm)
S1	PA1	0.506	5.74	5.68	1.6
	PA2	0.411	6.13	6.08	1.4
	PA3	0.347	6.01	5.96	1.5
S2	PA1	0.505	5.66	5.59	1.6
	PA2	0.410	5.98	5.92	1.5
	PA3	0.347	5.80	5.76	1.6
S3	010	0.501	1.57	1.53	5.8
	$1\bar{1}0$	0.392	1.95	1.92	4.7
	100	0.343	1.97	1.92	4.7
S4	010	0.503	2.05	2.01	4.4
	$1\bar{1}0$	0.392	2.49	2.45	3.7
	100	0.346	2.56	2.51	3.6
S5	010	0.504	1.99	1.94	4.6
	$1\bar{1}0$	0.392	2.70	2.66	3.4
	100	0.346	2.69	2.64	3.4
S6	011	0.505	2.74	2.70	3.3
	$1\bar{1}0$	0.393	3.13	3.09	2.9
	100	0.347	3.03	2.99	3.0

Table 7. Apparent crystallite thicknesses obtained from resolved meridional X-ray diffraction traces

Sample	Observed *d*-spacing (nm)	Experimental half-height width (2θ, deg)	Corrected half-height width (2θ, deg)	$L_{(hkl)}$ apparent crystallite size (nm)
S1	0.207	6.23	6.19	1.54
S2	0.207	5.56	5.53	1.72
S3	0.210	2.38	2.32	4.01
S4	0.210	2.41	2.37	4.01
S5	0.210	2.45	2.40	3.96
S6	0.210	2.60	2.56	3.72

at least 12 laterally packed chains. Meridional diffraction trace in the $2\theta = 10$–$60°$ range shown in Figure 8(a) shows the contributions of the equatorial and off-meridional peaks labelled as PM1, PM2, PM3 and PM4. The meridional peak labelled as PM4 is broad and well-defined with a *d*-spacing of 0.207 nm close to the *d*-spacing of 0.21 nm indexed as $\bar{1}05$ planes of triclinic unit cell of crystalline structure. As shown in Table 8, X-ray crystallinity of this sample is found to be 36.2 %.

WAXS pattern of *partially oriented* (sample S2) shown in Figure 6(b) shows similar features to sample S1 except with

Table 8. Comparison of crystallinity values of original PET fiber samples evaluated from DSC, density, infrared spectroscopy and X-ray diffraction methods

Sample	DSC crystallinity χ_c(%)	Crystallinity from density χ_c(%)	IR crystallinity χ_c(%)	X-ray crystallinity χ_c(%)
S1	15.63	31.42	21.76	36.2
S2	17.36	33.42	27.00	38.3
S3	35.09	42.75	42.26	60.2
S4	40.86	48.33	44.44	70.0
S5	43.10	51.92	42.00	65.8
S6	40.30	41.25	40.00	69.6

enhanced lateral order and orientation as shown by the lower azimuthal spread of the broad equatorial scatter into the meridional region. The equatorial trace shown in Figure 7(b) can be resolved into at least three peaks labelled as PA1, PA2 and PA3. The corresponding *d*-spacings and the half-height widths are summarized in Table 6. The meridional trace of this sample shown in Figure 8(b) shows contributions from equatorial and off-meridional reflections labelled, again, PM1, PM2, PM3 and PM4. The results suggest an oriented non-crystalline structure containing so called micro-crystallites consisting of at least 15 laterally packed chains. Following the peak resolution, X-ray crystallinity of this sample is found to be 38.3 %. It shows that increasing orientation along the fiber axis directions leads to an increased lateral order and the corresponding increase in the number of laterally packed chains.

Structure of Untextured Melt-Spun Yarns with High Orientation and Crystallinity

WAXS pattern of *fully oriented yarn* (sample S3) shown in Figure 6(c) shows fully developed crystalline structure with relatively enhanced crystalline orientation as shown by the intensity, sharpness and lower azimuthal arcing of the equatorial and off-equatorial reflections. The equatorial trace shown in Figure 7(c) can be resolved into at least three crystalline peaks indexed as 010, $1\bar{1}0$ and 100 peaks. The corresponding *d*-spacings, half-height widths and crystallite sizes are summarized in Table 6. The results suggest crystallite sizes perpendicular to the (010), ($1\bar{1}0$) and (100) planes as 5.8, 4.7 and 4.7 nm, respectively, corresponding to oriented 168 laterally packed chains along the fiber axis direction. Meridional trace of this sample is shown in Figure 8c. This peak has a *d*-spacing of 0.21 nm and is the azimuthal spread of $\bar{1}05$ reflection intersecting the meridional region. Crystallite thickness of this peak corresponds to at least 4 chemical repeat units (see Table 7). As shown in Table 8, the X-ray crystallinity for this sample is found to be 60.2 %.

WAXS pattern of *fully drawn yarn* (sample S4) shown in Figure 6(d) shows similar features to sample S3 with well-developed and oriented crystalline structure. The equatorial trace of this sample shown in Figure 9(a) can also be resolved into three crystalline peaks indexed as 010, $1\bar{1}0$ and 100 peaks. The corresponding *d*-spacings, half-height widths

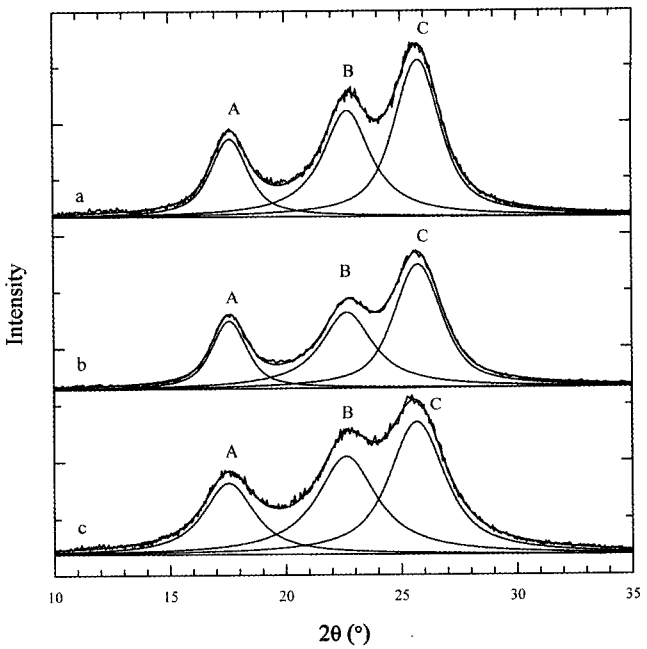

Figure 9. Resolved equatorial X-ray diffraction traces of (a) sample S4, (b) sample S5 and (c) sample S6. A: 010, B: $1\bar{1}0$, C: 100 peaks. See Table 1 for sample definition.

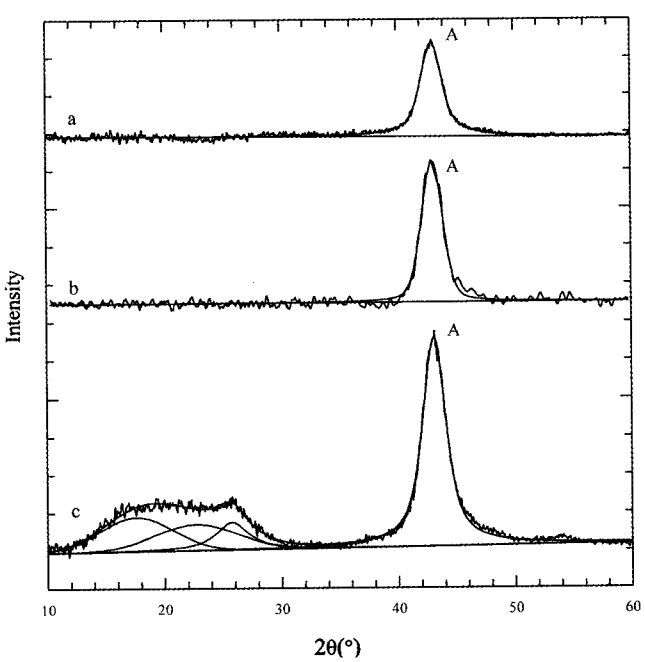

Figure 10. Resolved meridional X-ray diffraction traces of (a) sample S4, (b) sample S5 and (c) sample S6. A, extension of $\bar{1}05$ peak into the meridional region. See Table 1 for sample definition.

and apparent crystallite sizes are summarized in Table 6. The results suggest crystallite sizes perpendicular to the (010), ($1\bar{1}0$) and (100) planes as 4.4, 3.7 and 3.6 nm, respectively, corresponding to oriented 90 laterally packed chains along the fiber axis direction. The X-ray crystallinity for this sample is found to be 70 %. The results obtained from the resolution of meridional peak located at 0.210 nm, shown in Figure 10(a) and Table 7, suggest at least 4 repeating units. The results point to the fact that increasing alignment of chains leads to the improvement in the lateral order as shown by the increased number of chains in the laterally packed crystalline material.

Structure of Textured Melt-Spun Yarns with High Orientation and Crystallinity

WAXS patterns shown in Figure 6(e) and 6(f) of intermingled (sample S5) and air-textured (sample S6) yarns show well-developed crystalline structure with considerable azimuthal spread. The corresponding equatorial traces shown in Figure 9(b) and 9(c) can be resolved into three crystalline peaks. The corresponding *d*-spacings, half-height widths and apparent crystallite sizes are summarized in Table 6. The results suggest a crystalline structure containing at least 90 and 63 laterally packed chains for the intermingled and air-textured yarns. The X-ray crystallinity for the intermingled and air-textured yarns are 65.8 and 69.6 %, respectively (Table 8). The results obtained from the resolution of meridional peak located at 0.210 nm, shown in Figures 10(b) and 10(c), suggest at least 4 repeating units. Due to the effects of cold air-turbulance and the resulting possible mechanical deformation, the intermingled and air-textured samples possess somewhat lower number of laterally packed chains than the *fully oriented yarn* and *fully drawn yarn* samples.

Unpolarized Infrared Spectroscopy Data

Yazdanian *et al.* working on the oriented fibers of PET showed that the IR peaks at 962, 973 and 978 cm^{-1} can be assigned to the *trans* conformations of ethylene glycol units [2]. They also showed a direct relationship between the crystallinity measurements and the 973 cm^{-1} *trans* band concentration for both melt-spun and drawn fibers. In the same study, the amorphous phase is found to contain both *trans* and *gauche* conformations, whereas the crystalline regions are found to contain only *trans* conformations of ethylene glycol units. Therefore, in the present investigation, the 973 cm^{-1} *trans* band is chosen for the determination of the infrared crystallinity.

In a separate investigation, Ward and Wilding showed that the IR bands at 1410, 1018 and 874 cm^{-1} show no sensitivity to annealing effects [3]. Therefore, one of these bands can be chosen as an internal band. In the present study, the IR peak at 1018 cm^{-1} due to the proximity to the 973 cm^{-1} *trans* band is chosen as an internal standard band to normalize the absorbance values.

The infrared crystallinity index values are determined using equation (12) after obtaining the absorbance values

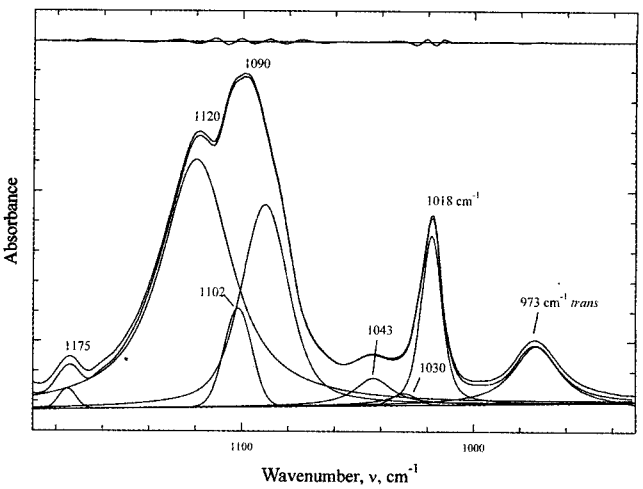

Figure 11. An example of the unpolarized IR spectrum peak resolution in the 1190–930 cm^{-1} region corresponding to sample S3. The lower curves are the fitted peaks, the middle curve is the observed spectrum and the upper curve is the difference between the observed spectrum and the fitted spectrum on the same scale.

Table 9. Comparison of crystallinity values of annealed samples evaluated from DSC, density and infrared spectroscopy

Annealing time	DSC crystallinity χ_c(%)	Crystallinity from density χ_c(%)	IR crystallinity χ_c(%)
Unannealed	15.63	33.42	21.76
1 hour	36.34	41.25	38.54
2 hours	36.59	42.75	43.39
5 hours	35.68	47.58	42.18
7.5 hours	40.58	51.90	44.03
120 hours	40.48	51.08	41.86

from the curve fitting of 1190–930 cm^{-1} region shown in Figure 11. The infrared crystallinity values for the melt-spun untextured samples (i.e., samples S1-S4) and textured samples (samples S5 and S6) are summarized in Table 8 and in Table 9 for the annealed samples.

The results show that the infrared crystallinity values increase in line with the increases in the molecular orientation along the fiber axis direction. The same trend also exists for the annealed samples.

As shown in Figures 12 and 13, there is a relationship between the crystallinity values measured by different techniques and the optical orientation parameter, $\langle P_{200} \rangle_{opt}$ for the untextured, textured and annealed samples.

Comparison of Crystallinity Values Obtained via Different Methods

By definiton, the crystallinity is defined as the relative amount of three dimensionally ordered structure and is usually most

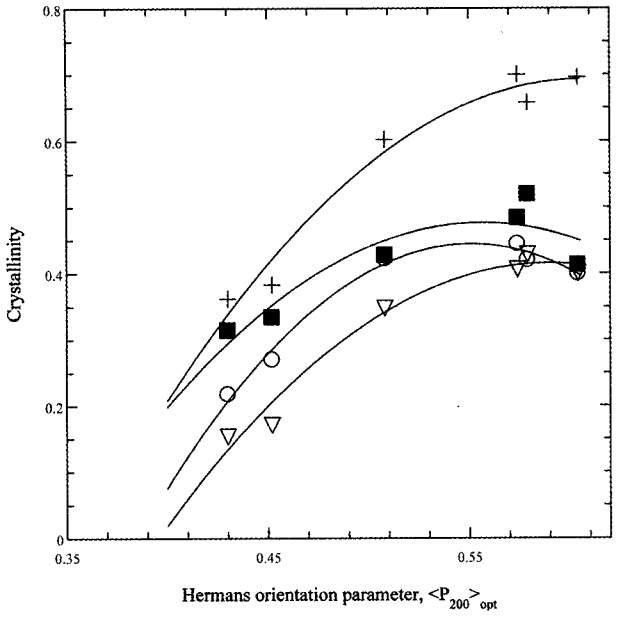

Figure 12. The relationship between the optical orientation parameter, $<P_{200}>_{opt}$ and the crystallinity values of original samples obtained from different methods. (▽) DSC, (○) IR, (■) density, (+) X-ray.

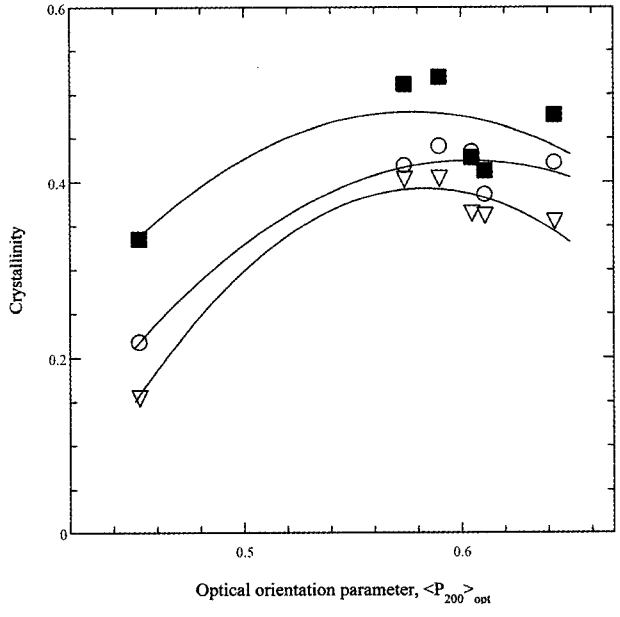

Figure 13. The relationship between the optical orientation parameter, $<P_{200}>_{opt}$ and the crystallinity values of annealed samples obtained from different methods. (▽) DSC, (○) IR, (■) density.

directly measured by wide-angle X-ray diffraction. Although the numerical results summarized in Tables 8 and 9 and shown in Figures 12 and 13 show that the crystallinity values obtained from density, thermal analysis, infrared spectroscopy and X-ray methods are different, but they are found to correlate reasonably well with each other shown in Figures 14 and 15. The crystallinity values obtained from the thermal analysis are found to be on the lowest side and the values obtained from X-ray diffraction are, on average, on the highest side. The crystallinity values obtained from the density and infrared spectroscopy fall between these two limits. Basically, the X-ray diffraction method using the equatorial region measures the lateral order between a predefined 2θ region and is based on the separation of oriented crystalline and unoriented non-crystalline (i.e., amorphous) scatter by curve-fitting procedure. Although the X-ray procedure is more reliable than the other methods of measuring crystallinity but the X-ray crystallinity may contain small amounts of oriented non-crystalline material, but this quantity is not expected to be more than 5–10 %.

In the case of infrared spectoscopy, the crytallinity values are based on the *trans* conformer content in the crystalline phase. Assuming further contributions of *trans* conformer content in the amorphous phase, there is no doubt that, the total trans conformer content is expected to be ever higher.

The crystallinity values determined from density assumes a constant crystalline and amorphous density values. It is well known that the amorphous density increases following the introduction of orientation during the fiber production and the drawing stages. The crystallinity values for the samples with low orientation such as *medium oriented* (sample S1) and *partially oriented* (sample S2) yarns may be acceptable due to small changes in the amorphous density values, whereas the samples with higher orientation may have slightly unreliable crystallinity values determined from density.

The main shortcomings of the thermal analysis are mainly cold-crystallization taking place before the melting process and the uncertainties in establishing the baselines for the calculation of integrated areas. Although the crystallization exotherm is deducted from the melting endotherm but the uncertainty still remains in the correct positioning of the baselines for area integration. The uncertainty becomes considerably higher when a baseline arbitrarily placed between the crystallization exotherm and melting endotherm for the samples with low crystallinity.

The crystallinity values shown in Figures 14 and 15 are used for the evaluation of linear correlation coefficient (R) after drawing the best fit lines using linear least-squares method. The results show a reasonable correlation between X-ray crystallinity and DSC crystallinity with $R = 0.98$ for the original samples shown in Figure 14(b). There are also reasonable correlation between X-ray crystallinity and infrared crystallinity values with $R = 0.96$ shown in Figure 14(c) and between infrared crstallinity and DSC crystallinity with $R = 0.96$ shown in Figure 14(e). As far as the combined data from original and annealed samples are concerned, the best correlation is observed between the infrared crystallinity and

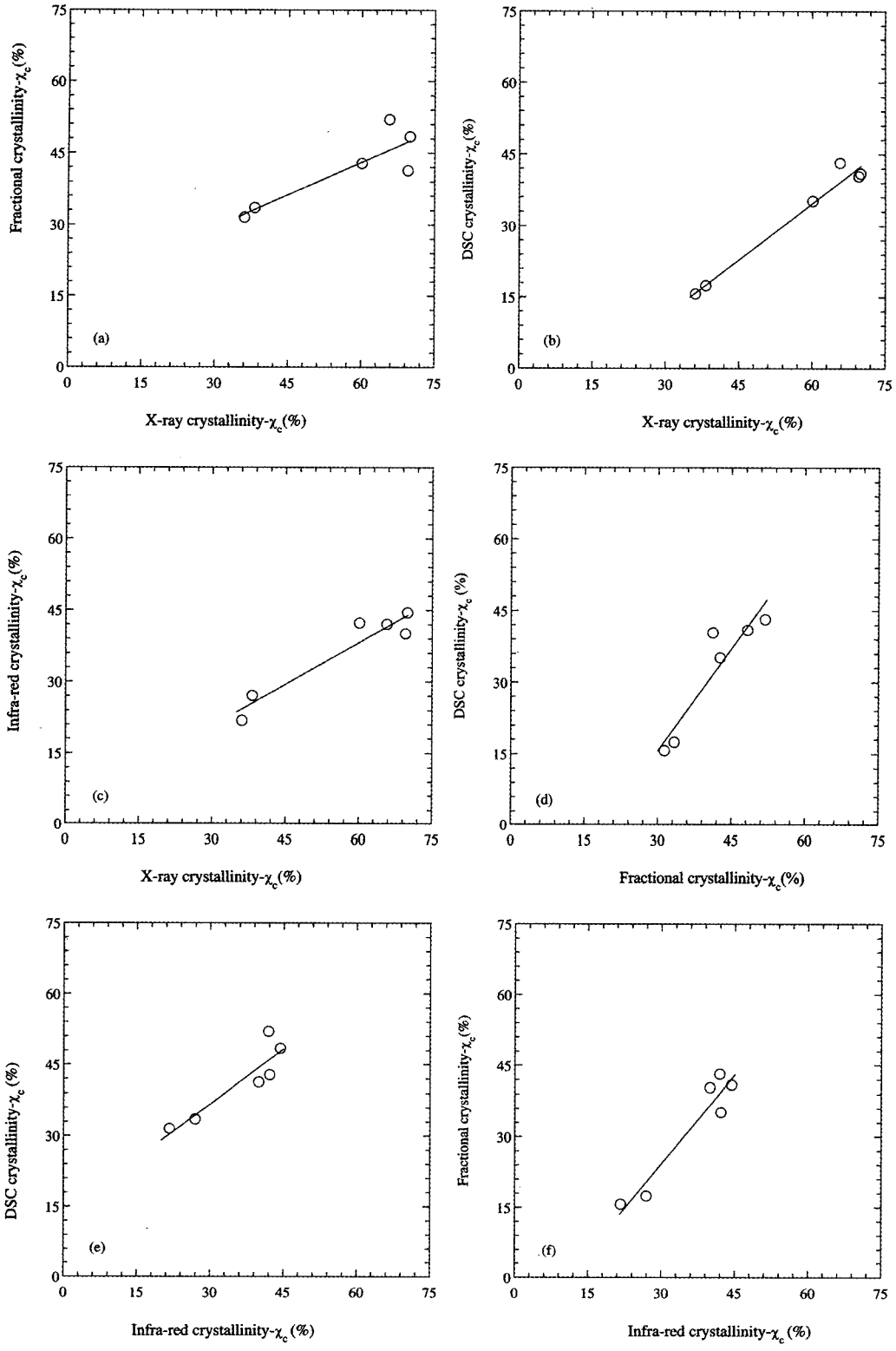

Figure 14. Correlation between crystallinity values obtained via different methods for the original samples listed in Table 1. A linear least-squares fitted line is drawn through the points. Linear correlation coefficient (R) of the plots are given as follows: (a) X-ray crystallinity vs. crystallinity from density measurement (R = 0.87), (b) X-ray crystallinity vs. DSC crystallinity (R = 0.98), (c) X-ray crystallinity vs. infrared crystallinity (R = 0.98), (d) fractional crystallinity vs. DSC crystallinity (R = 0.93), (e) infrared crystallinity vs. DSC crystallinity (R = 0.96), (f) infrared crystallinity vs. fractional crystallinity (R = 0.90).

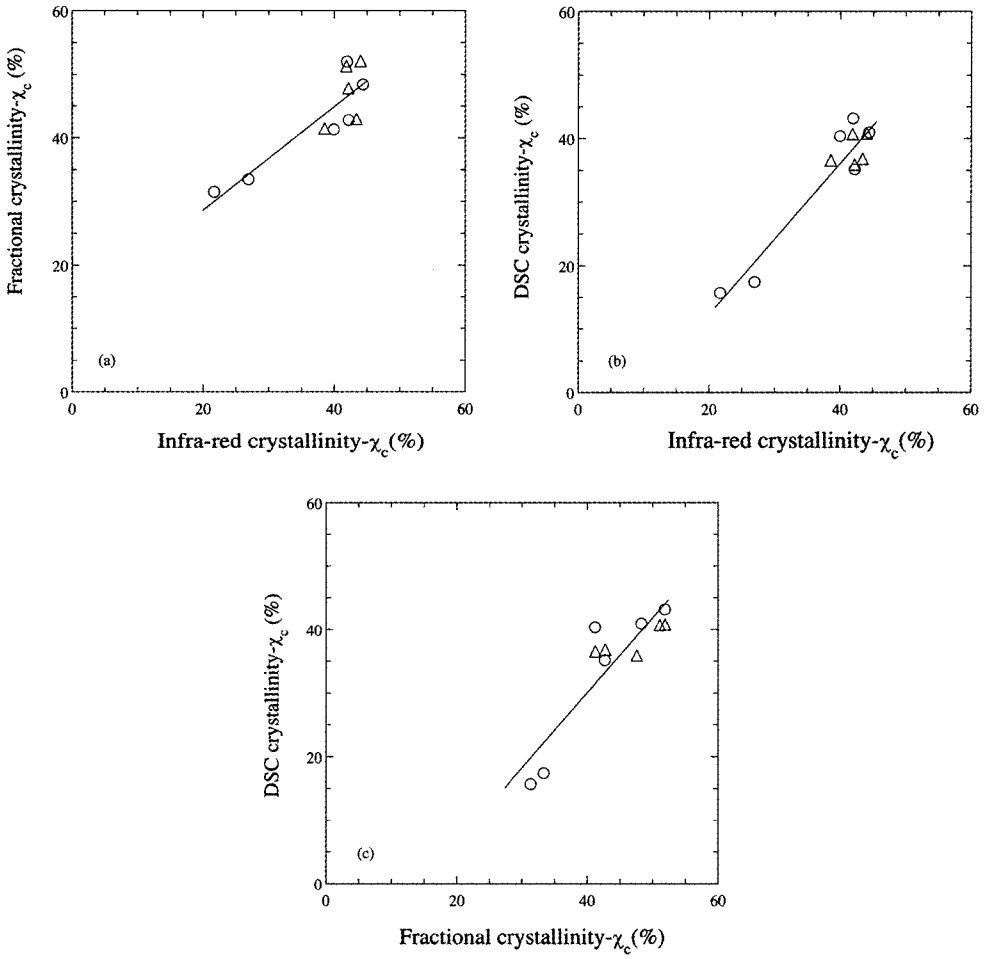

Figure 15. Correlation between crystallinity values obtained via different methods for the combination of original and annealed samples. A linear least-squares fitted line is drawn through the points. Linear correlation coefficient (R) of the plots are given as follows: (a) infrared crystallinity vs. fractional crystallinity (R = 0.86), (b) infrared crystallinity vs. DSC crystallinity (R = 0.94), (c) fractional crystallinity vs. DSC crystallinity (R = 0.89). (○) original samples listed in Table 1, (▽) annealed samples listed in Table 3.

DSC crystallinity with R = 0.94 shown in Figure 15(b).

Scanning Electron Microscopy Observations

The surface features of the PET fiber samples were investigated using an ISI-100A Scanning Electron Microscope with a voltage setting of 5 kV and a specimen to detector distances ranging between 8 mm to 12 mm, respectively. As shown in Figure 16, the lateral image of *medium oriented fiber* (sample S1) characterized by low orientation shows micro-cracks on the fiber surfaces becoming smooth on surfaces of the *highly oriented fiber* as shown in Figure 17. A typical lateral image of a knotted *medium oriented fiber* shown in Figure 18, shows kinking bands across the fiber and excellent bending characteristics without the presence of delamination or fibrillation often seen in rigid-rod polymer systems indicating the suitability for an easy fabric formation. The kinking is found to disappear with highly oriented samples.

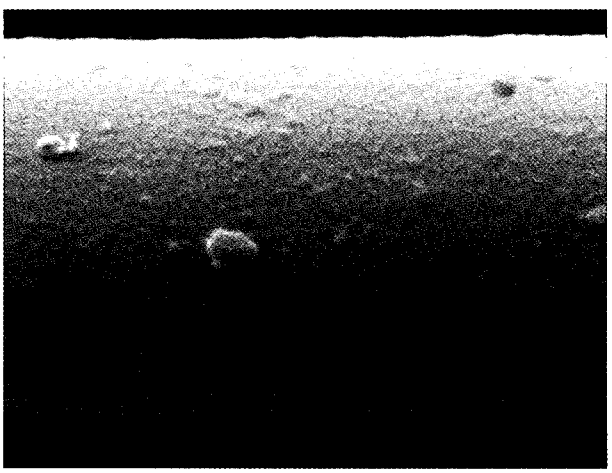

Figure 16. Longitudinal SEM image of *partially oriented fiber* showing micro-cracks along the fiber axis direction (×10,000).

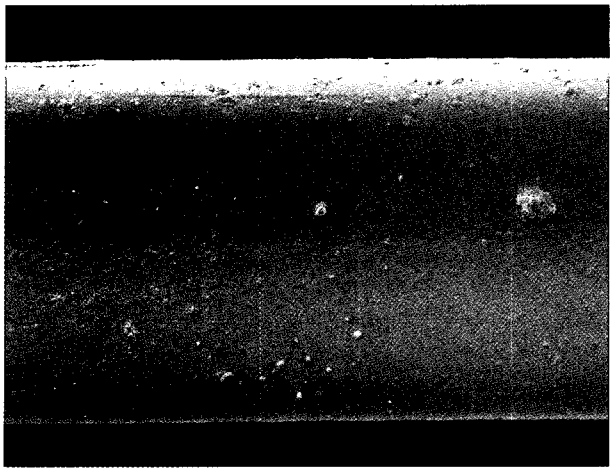

Figure 17. Longitudinal SEM image of *fully oriented fiber* showing smooth surface along the fiber axis direction (×10,000).

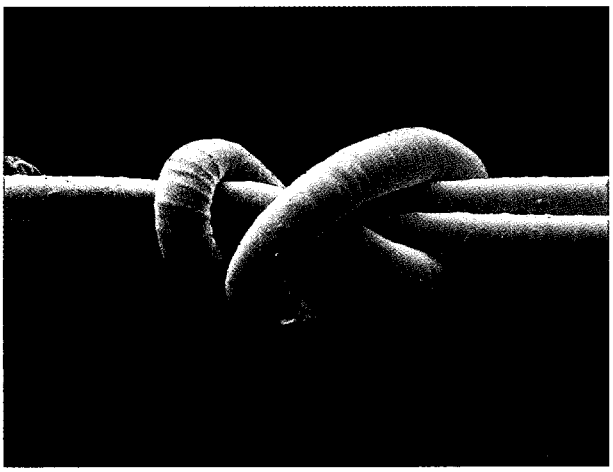

Figure 18. Longitudinal SEM image of *medium oriented fiber* with a knot showing kinking bands across the fiber (×1,000).

Conclusions

The quantitative measurement of crystallinity, crystallite size and orientation parameters of a selection of commercially available poly(ethylene terephthalate) fibers have been carried out using wide-angle X-ray diffraction, infrared spectroscopy, thermal analysis and optical microscopy techniques. Annealing experiments carried out under constrained conditions at a fixed temperature for various times showed enhanced molecular orientation and crystallinity as shown by the increased values of birefringence and melting enthalpies.

Optical microscopy has been used to obtain birefringence values as a means of overall orientation via the refractive index measurements. The birefringence and refractive index values are found to decrease with increasing wavelength of light used in the experiments. Data from thermal analysis, infrared spectroscopy, X-ray diffraction and density values obtained from the samples used for the isotropic refractive index measurements are used for the determination of crystallinity values. The measured crystallinity values are found to be different, but they are found to correlate reasonably well with each other. The crystallinity obtained from the density measurement is found to be less reliable with the highly oriented samples due to the assumption of constant amorphous density used in the calculations, whereas the crystallinity calculated from the X-ray diffraction measurement is found to be more reliable. The results suggest a close relationship between increasing overall orientation and increasing crystallinity as a direct result of increasing processing speeds and annealing procedure under constrined condition.

The results from X-ray diffraction analysis show that the samples with relatively low orientation possess oriented non-crystalline array of chains, whereas those with high molecular orientation possess well defined and oriented crystalline array of chains along the fiber axis direction. Crystallite size values are found to increase with increasing molecular orientation due to the increasing perfection of lateral order. It shows that, possibly, due to the mechanical deformation taking place during the intermingling and air-texturing processes, the lateral order for these samples, appear to be less well ordered than the fully oriented and fully drawn yarn samples.

SEM examination of surface features of samples showed surface irregularities characterized by micro-cracks along the fiber axis direction with samples of low orientation becoming smoother with samples of higher orientation. All the samples showed excellent bending behavior when knotted implying relatively easy fabric formation.

Further studies on the use of high temperature infrared spectroscopy and X-ray diffraction as a function of temperaturee before, during and after melting would enhance our understanding of the processes taking place. Use of TEM for the direct measurement of crystallite size would be helpful for the assessement of the apparent crystallite size obtained from X-ray diffraction analysis.

Acknowledgements

The author would like to thank Polyteks A.S. of Turkey for the supply of the samples investigated in the present study. Thanks also go to Pinar Tasdelen and Alison Edmed for the assistance with the data collection. The help and assistance of Trevor Jones of Department of Textiles of UMIST (UK) is very much appreciated with the SEM images. Ian Brough of Materials Science Centre of UMIST (UK) is very much appreciated for his assistance with the X-ray diffraction work. Special thanks go to an anonymous reviewer for making useful comments.

References

1. D. A. Jarvis, I. J. Hutchinson, D. I. Bower, and I. M. Ward,

Polymer, **21**, 41 (1980).
2. M. Yazdanian, I. M. Ward, and H. Brody, *Polymer*, **26**, 1779 (1985).
3. I. M. Ward and M. A. Wilding, *Polymer*, **18**, 327 (1977).
4. J. Guevremont, A. Ajji, K. C. Cole, and M. M. Dumoulin, *Polymer*, **36**, 3385 (1995).
5. B. J. Holland and J. N. Hay, *Polymer*, **43**, 1835 (2002).
6. N. Everall, D. MacKerron, and D. Winter, *Polymer*, **43**, 4217 (2002).
7. Y. Zhang, Y. Lu, Y. Duan, J. Zhang, S. Yan, and D. Shen, *J. Polym. Sci.: Polym. Phys.*, **42**, 4440 (2004).
8. Y. Zhang, Y. Lu, S. Yan, and D. Shen, *Polymer J.*, **37**, 133 (2005).
9. R. A. Hujts and S. M. Paters, *Polymer*, **35**, 3119 (1994).
10. J. I. Purvis, D. I. Bower, and I. M. Ward, *Polymer*, **14**, 398 (1973).
11. D. I. Bower and I. M. Ward, *Polymer*, **23**, 645 (1982).
12. G. Farrow and D. Preston, *Brit. Polym. J.*, **11**, 353 (1960).
13. A. M. Hindeleh and D. J. Johnson, *Polymer*, **19**, 27 (1978).
14. J. K. Keum and H. H. Song, *Polymer*, **46**, 939 (2005).
15. Y. Miwa, Y. Takahashi, Y. Kitano, and H. Ishida, *J. Mol. Struct.*, **441**, 295 (1998).
16. Y. Yoshioka, M. Tsuji, Y. Kawahara, and S. Kohjiya, *Polymer*, **44**, 7997 (2003).
17. I. Karacan, A Taraiya, D. I. Bower, and I. M. Ward, *Polymer*, **34**, 2691 (1993).
18. I. Karacan, D. I. Bower, and I. M. Ward, *Polymer*, **35**, 3411 (1994).
19. A. M. Hindeleh, D. J. Johnson, and P. E. Montague in "Fiber Diffraction Methods", ACS Symp. No. 141 (A. D. French and K. H. Gardner Eds.), p.149, American Chemical Society, Washington DC, 1983.
20. A. R. Stokes, *Proc. Phys. Soc.*, **A166**, 283 (1948).
21. H. de Vries, *Colloid & Polym. Sci.*, **257**, 226 (1979).
22. R. de P. Daubeny, C. W. Bunn, and C. J. Brown, *Proc. Roy. Soc. (London)*, **A226**, 531 (1954).
23. B. Wunderlich, "Macromolecular Physics", Vol. 3, pp.68-69, Academic Press, New York, 1980.
24. A. Demir, *Textile Asia*, **21**, 114 (1990).
25. Z. D. Jastrzebski in "Encyclopedia of Polymer Science and Technology", (H. F. Mark, N. G. Gaylord, and N. M. Bikales Eds.), Vol. 2, p.138, Wiley Interscience, New York, 1965.